Proceedings of ASME 2015 Pressure Vessels & Piping Division Conference
ASME/PVP 2015
July 19-23, 2015, Boston, USA

PVP2015-45296

BUCKLING OF A FLAT PLATE IN A CONFINED AXIAL FLOW

Julie Adjiman
IMSIA
UMR CNRS EDF CEA ENSTA 8193
Clamart, 92141
France
Email julie.adjiman@ensta-paristech.fr

Olivier Doaré
IMSIA
UMR CNRS EDF CEA ENSTA 8193
Palaiseau, 91120
France
Email olivier.doare@ensta-paristech.fr

Pierre Moussou
EDF R&D
Clamart, 91120
France
Email pierre.moussou@edf.fr

ABSTRACT

Static instability of flexible structures forced by a parallel flow, a.k.a. divergence, has been the subject of a relatively small amount of studies, unlike flutter. In order to prepare future studies of the collective behaviour of several slender structures coupled by the fluid in axial flow, the canonical case of a flat flexible plate clamped at both ends is investigated numerically and experimentally. The onset of divergence is determined throughout a series of calculation of the fluid forces generated by a prescribed deformation of the plate. Using the Galerkin method, these fluid forces are expanded in the basis of the natural modes; they exactly balance the mechanical forces when the fluid velocity reaches the instability threshold. The instability velocity can be determined by an eigenvalue calculation involving the fluid force expansion and the modal stiffnesses of the plate. Comparisons are provided with 2D analytical calculations and with an experiment performed with a 0.3m$\times$0.03m mylar plate at Reynolds numbers varying between 10^4 *and* 10^5*. A fair agreement is observed between the 3D potential calculation and the experiments, whereas the 2D analytical solution underestimates the instability velocity by a factor higher than 2.*

NOMENCLATURE

- C plate-to-wall distance along the y axis
- D plate-to-wall distance along the z axis
- E Young modulus of the plate
- H plate's width
- h_p plate's thickness
- K_n wavenumber associated to the n-th mode of the plate
- L plate's length
- p fluid pressure
- U inlet fluid velocity
- ν Poisson ratio
- Φ potential function associated to the fluid flow
- ρ volumic mass of the fluid

INTRODUCTION

When a slender deformable structure is placed in an axial flow, the straight equilibrium position becomes unstable once a critical flow velocity is reached. The instability can be of the buckling or flutter type. In the first case, the structure deformation undergoes exponentially growing until non-linearities act so that the structure reaches a new static equilibrium position. In the case of flutter instability, exponentially growing oscillations occur until a steady regime is obtained. The type of instability, buckling or flutter, is mainly influenced by the structural boundary conditions [1, 2] and the present work focuses on buckling type instabilities of clamped-clamped structures, which occur in high speed travelling plates in the printing industry [3], aeronautics [4] and flat-type fuel assemblies in research nuclear reactors [5].

Buckling of slender cylinders has been investigated in [6]; 3-dimensional effects in a channel flow have been studied theoretically [7] and experimentally [8] in the context of flag flutter, but still have to be addressed in the context of buckling.

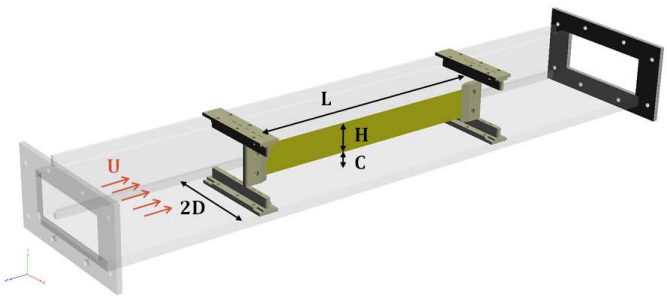

FIGURE 1. NOTATIONS

In this paper, the case of a single structure clamped at both ends is considered with a focus on the influence of lateral confinement. First, the general equations of potential flow are derived in order to estimate the aerodynamic efforts exerted on a statically deformed plate. Then, a Galerkin method in the basis of natural clamped-clamped modes brings out the equilibrium between the fluid and mechanical forces at the precise flow velocity associated with the onset of divergence. Calculations are performed in both 2D and 3D; comparisons with experimental data are provided for several wall-to-plate distance $\frac{D}{L}$ values.

THEORETICAL BACKGROUND

Structure equations

In this work, a plate of length L, width H is placed in a rectangular channel of dimensions $H+2C$ and $2D$, as sketched in Fig.(1). The lateral plate deflection ζ is supposed to depend only on the axial coordinate x. It is governed by the linearized plate equation taking into account the effect of an external force density f_{ext} [9, 10] :

$$\frac{Eh_p^3}{12(1-\nu^2)}\left(\frac{\partial^2}{\partial x^2}+\frac{\partial^2}{\partial z^2}\right)^2\zeta = f_{ext}, \tag{1}$$

where ν and E are respectively Poisson's ratio and Young's modulus of the plate, and h_p is the plate's thickness.

The natural modes are of widespread use in flutter analysis [7,11], and they can be used in divergence cases as well [4,12] Expanding the structure linear equation on the basis of natural modes, in a static context, is a choice motivated by practical considerations: the differential operator in Eq. (1) is replaced by a multiplication by the 4^{th} power of the wavenumber.

The plate deflection due to an external force density can indeed be expressed as a combination of the mode shapes, i.e. $\zeta(x,t)=\sum_n q_n\xi_n$. Equation **??** then reads,

$$\frac{Eh_p^3}{12(1-\nu^2)}\sum_n K_n^4 q_n\xi_n = f_{ext} \tag{2}$$

where q_n, referred to as the n^{th} modal displacement, has the dimension of meters. Eq. (2) comes in handy if the force density can also be expanded in the basis of the natural modes as discussed in a further section.

Fluid equations

In the reference state where the plate remains undeformed, the flow potential is equal to Ux, which ensures that the velocity is uniform and directed toward x. A prescribed bending of the plate modifies the flow pattern, and the corresponding potential can be denoted $Ux+\Phi$. The potential function Φ fulfills the Laplace equation so that mass is conserved, and its boundary conditions can be written $\mathbf{grad}\,\Phi.\mathbf{n}=0$ at the inlet and the outlet of the rig, and also along its surrounding walls. The boundary condition along the deformed plate requires some more care: it stipulates that the total flow velocity $\mathbf{U}+\mathbf{grad}\Phi$ is parallel to the deformed plate. In the framework of small perturbations, this condition is referred to as the linearized permeability condition [13, 14]:

$$\frac{\partial\Phi}{\partial z}-U\frac{\partial\zeta}{\partial x}=0 \tag{3}$$

namely, the sum of the z component of the perturbation and of the unperturbed flow multiplied by the x component of the normal vector to the plate vanishes.

Expanding the plate deformation is terms similar to the ones of Eq. (2), the potential Φ is expanded in:

$$\Phi = U\sum_n q_n\varphi_n \tag{4}$$

each dimensionless potential φ_n fulfilling the Laplace equation,

$$\Delta\varphi_n = 0, \tag{5}$$

with boundary conditions,

$$\frac{\partial\varphi_n}{\partial z}=\frac{\partial\xi_n}{\partial x} \quad \text{on the plate,} \tag{6}$$

$$\frac{\partial\varphi_n}{\partial\mathbf{n}}=0 \quad \text{on the channel walls.} \tag{7}$$

To further on, the pressure field generated by the fluid can be determined with the help of the steady Bernoulli equation. At the first order, the perturbed pressure is:

$$p = -\rho U \frac{\partial \Phi}{\partial x} = -\rho U^2 \sum_n q_n \frac{\partial \varphi_n}{\partial x} \tag{8}$$

Eqs. (4), (6) and (8) summarize the resolution of the fluid equations under the effect of a prescribed deformation of the plate.

Fluid forces in the basis of plate modes

For a prescribed deflection $q_p \xi_p$ of the plate proportional to the p^{th} mode shape, Eq. (8) shows that the pressure fields on both sides of the plate generate a force distribution equal to:

$$f_p = \rho U^2 q_p \frac{\partial}{\partial x}(\varphi_p^+ - \varphi_p^-), \tag{9}$$

where φ_p^- and φ_p^+ are the potentials on each side of the plate .

It is now assumed that the derivatives of the potentials $\varphi_p^\pm$ along the plate can be expanded in the basis of the natural modes. A convenient way to determine the coefficients in such an expansion consists in introducing cross-integrals of the mode shapes and of the function considered. As an illustration, an arbitrary function $g(x,y)$ should be expanded in:

$$g(x,y) \approx \sum_p \frac{\int g \xi_p ds}{\int \xi_p^2 ds} \xi_p(x,y) \tag{10}$$

where the normalisation term $\int \xi_p^2 ds$ is required to ensure that the above procedure leaves any basis function ξ_n invariant. The integral ratios in the r.h.s. term of Eq. (10) define in a unique manner the coefficients of any function g expanded in the basis of the mode shapes ξ_p. Introducing the length L of the plate for dimensional consistency, this procedure can be applied to the pressure forces:

$$f_p = \rho U^2 \frac{q_p}{L} \sum_n H_{pn} \xi_n,$$
$$\text{where } H_{pn} = \frac{L}{\int \xi_n^2 ds} \int \frac{\partial}{\partial x}(\varphi_p^+ - \varphi_p^-) \xi_n \, ds. \tag{11}$$

This equation highlights the fact that the fluid forces, due to a modal deformation ξ_p, generate secondary deformations involving other modes. The accuracy of such an expansion may be questioned close to the plate ends where every mode shape vanishes, yet this discrepancy should not have effects upon the mode deflection nor the divergence threshold, as a force applied in the vicinity of a fixed point does not generate a large deflection. An illustration of this is provided in Appendix B: it holds reasonably well for values of the reduced wall-to-plane distances lower than 0.25. Consistency of this approach was tested by examining the convergence of the unstable mode and of the threshold velocity with the number of modes.

Fluid structure coupling in the basis of plate modes

Merging the previous sections, the onset of divergence can now be investigated: it is defined as the exact balance of the plate stiffness force by the fluid force. In mathematical terms, this situation occurs when a non-vanishing solution of the fluid-structure equations exists. Let for that purpose Eq. (11) be combined to the plate equation (2). The onset of instability is associated with a non-vanishing solution of:

$$\frac{E h_p^3}{12(1-\nu^2)} \sum_n K_n^4 q_n \xi_n = \rho U^2 \sum_p \left(\frac{q_p}{L} \sum_n H_{pn} \xi_n \right) \tag{12}$$

Rearranging the terms, and equating the coefficients of ξ_n, one gets:

$$\frac{1}{12(1-\nu^2)} \frac{E}{\rho U^2} \frac{h_p^3}{L^3} (K_n L)^4 q_n = \sum_p H_{pn} q_p \tag{13}$$

Considering q_p as a the components of a state vector $\mathbf{V}$, this equation can be rewritten in matrix form by introducing a diagonal matrix $\mathbf{K_4}$, the coefficients of which being the dimensionless terms $K_n L$ elevated to the fourth power, and a matrix $\mathbf{H}$ with coefficients along the p-th lines and the n-th rows equal to H_{pn}:

$$\frac{1}{12(1-\nu^2)} \frac{E}{\rho U^2} \frac{h_p^3}{L^3} \mathbf{V} = \mathbf{K_4^{-1} H V} \tag{14}$$

For any deformation, the two matrices $\mathbf{K_4}$ and $\mathbf{H}$ give the flexural rigidity force and the pressure force in competition associated to the deformation in the basis of natural modes. Writing the physical problem as in Eq. (14) introduces a specific fluid velocity for which a non-straight deformation of the plate exists and such that the fluid and structure forces are exactly equal: for a specific value of the fluid velocity, the system is on the verge of instability. Divergence therefore occurs when the velocity U is such that there is a non-trivial solution to Eq. (14), *i.e.* when the ratio in the l.h.s. term of Eq. (14) coincides with an eigenvalue of the matrix $\mathbf{K_4^{-1} H}$.

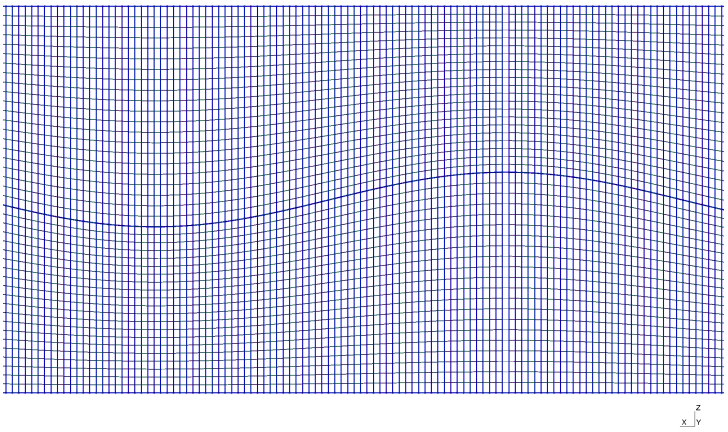

FIGURE 2. PARTIAL CUT VIEW OF THE MESH ALONG IN THE X-Z PLANE

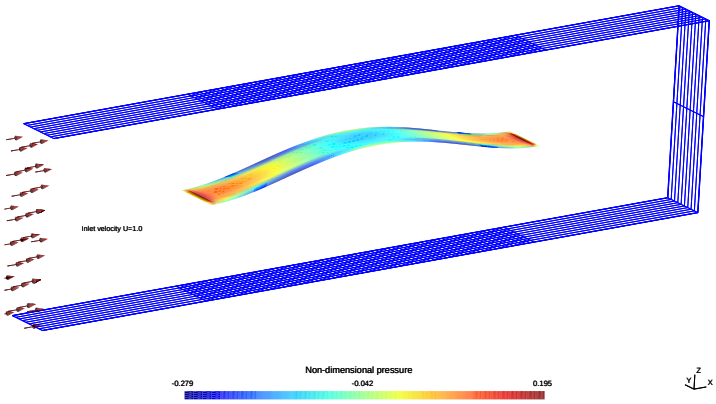

FIGURE 3. DIMENSIONLESS PRESSURE ON THE UPPER SIDE OF THE PLATE WITH A FIRST MODE SHAPE AND PROFILE OF THE INLET VELOCITY

$$U_{crit} = U\sqrt{\rho\frac{L^3}{h_p^3}\frac{12(1-\nu^2)}{E}} = \sqrt{\frac{1}{eigenvalues(\mathbf{K_4^{-1}H})}} \quad (15)$$

Numerical computation of the 3-dimensionnal flow potential

The fluid problem (5) with boundary conditions (6-7) is solved numerically for a 3-dimensional geometry, as sketched in Fig.(1). For the sake of comparison, an analytical derivation of the solution for a 2D problem is shown in appendix A. The plate is included in a 3D 'fluid box'; the plate is built with a small thickness, which allows to have a clear separation between the two faces of the plates. The inlet velocity profile is uniform in this x direction; at the outlet, the condition $\Phi = 0$ is applied. On the lateral walls of the box, an ideal slip condition is applied: $\mathbf{grad}\Phi.\mathbf{n} = 0$. The plate profile in the normal direction follows an analytical mode shape [15] with an amplitude ε, such that, with the notations introduced before, $\frac{q_p}{L} = \varepsilon$. The plate's profile is included in the Gmsh [16] generating script of the mesh, leading to a deformed plate as shown in Fig. 2. The plate's width is divided in 30 cells, and its length is divided in up to 200 cells such that each cell is close to a perfect square: this resolution allows to correctly discretize modes up to the fifth longitudinal order, and to generate volumic hexaedra cells, thanks to the default algorithm (named 'Delaunay' in Gmsh).

The stationary potential fluid flow is then computed in the fluid domain around the static deformed plate. As a first step, the potential problem $\Delta\Phi_p = 0$ is solved in the 'fluid box' with finite elements method implemented in the open-source software *Code_ Aster* [17], choosing $L = 1$ and $U = 1$. Then, the total velocity field is computed as the gradient of potential, and the pressure field is finally computed all over the fluid domain with Bernoulli's equation:

$$p_p = -\frac{1}{2}\rho(\nabla\Phi_p)^2 \quad (16)$$

This sequence is repeated for each mode number, and for several values of confinement.

In the second step, the fluid force exerted on the plate associated to a deformed plate in the p^{th} mode is computed as $f_p = -p_p^+ + p_p^-$, *i.e.* as the difference between the pressure on each face of the plate. The fluid forces are expanded in the modes basis in order to compute the coefficients in the matrices $\mathbf{K}$ and $\mathbf{H}$, such that:

$$H_{pn} = \frac{1}{\int \xi_n^2 ds}\int \frac{f_p}{\rho}\xi_n\, ds \quad (17)$$

As described earlier, the eigenvalues of the matrix $\mathbf{K_4^{-1}H}$ are finally computed, which therefore give the critical non-dimensional velocity for each mode.

EXPERIMENTS

A flexible plate is cut in a Mylar sheet (thickness $h_p = 250\mu m$, Young modulus $E = 5.2$ GPa, Poisson coefficient $\nu = 0.38$, length $L = 0.28$ m, width $H = 0.03$ m). In order to perform clamped-clamped boundary conditions, a streamlined piece is attached to both ends of the plate with crossing screws; the assembly is inserted and centered in a rectangular box made of transparent Plexiglas (inner dimensions: 0.04 m x 0.10 m). A fan with a honeycomb grid is connected to the box, which allows a uniform steady flow from 0 up to 50 m/s, measured with a Pitot tube

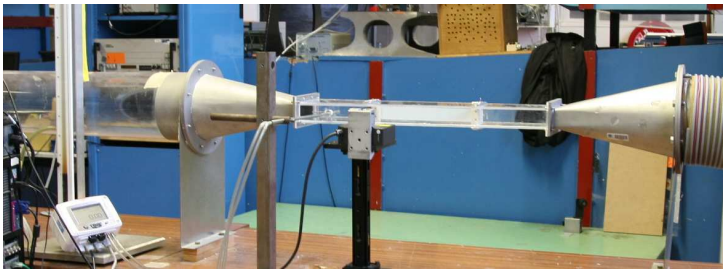

FIGURE 4. EXPERIMENTAL SET-UP: THE PLATE (IN WHITE) INSIDE THE PLEXIGLAS CELL CONNECTED TO THE AIR FAN; ON THE LEFT, A PITOT TUBE CONNECTED TO A PRESSURE SENSOR; IN THE FOREGROUND, THE LASER DISPLACEMENT SENSOR

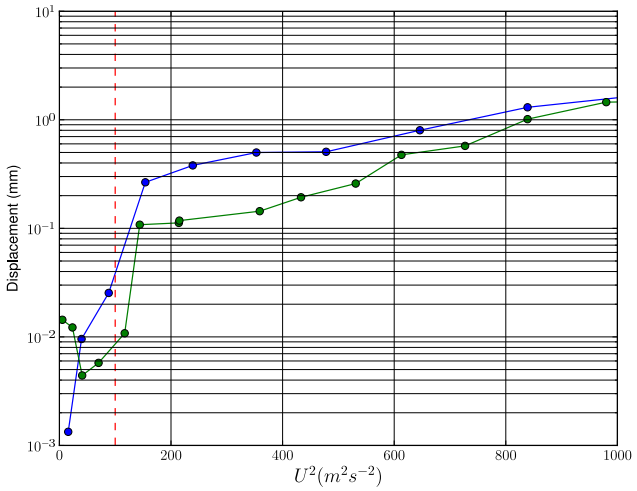

FIGURE 5. TWO MEASUREMENTS OF MEAN DISPLACEMENT AT 0.75L (D/L = 0.2). RED LINE: ESTIMATED DIVERGENCE THRESHOLD.

at the center of the box. A laser sensor is used to measure the deflection of the plate locally, giving access to the plate's shape and amplitude of deformation. Due to small fluctuations, the considered amplitude is the average over 10s of measurements at sampling rate 1kHz. At the same time, the spectrum density of the signal and the signal itself are checked to ensure that the variation does not exceed 5% of the average value.

In Fig.5 the mean displacement of a point at 0.75L in the flow direction is plotted against the square of measured inlet velocity. The divergence threshold is determined by the slope change; in this case, the critical velocity is approxiamtely 10 m/s, which gives a non-dimensional value $U_{div} \simeq 18$. The experimental value of the lateral confinement $\frac{D}{L}$ can be modified by joining small boards on to the walls; for three configurations ($\frac{D}{L}$ = 0.2, 0.1 and 0.05) the critical velocity has been determined

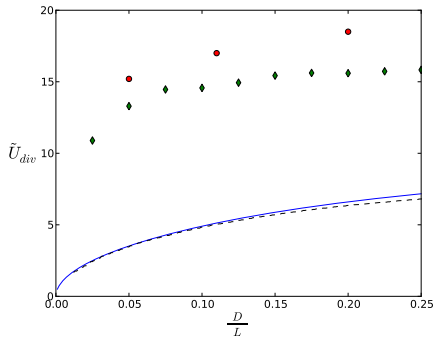

FIGURE 6. DIMENSIONLESS DIVERGENCE VELOCITY AS A FUNCTION OF THE WALL-TO-PLATE DISTANCE $\frac{D}{L}$. PLAIN LINE: ANALYTICAL 2D SOLUTION, DASHED LINE: GUO'S SOLUTION AS GIVEN IN [2], DIAMONDS: NUMERICAL 3D SOLUTION, RED DOTS: EXPERIMENTAL.

experimentally.

Fig.6 shows the evolution of critical divergence velocity for several values of the confinement parameter $\frac{D}{L}$. The 2D analytical model is in good agreement with Guo's solution as given in [2]; the critical velocities for divergence of the higher modes, not shown here, can be also computed with this 2D model; but these velocities can not be visualized experimentally, because the less stable mode (first mode here) would have to be prevented from diverging, in order to see the next mode's divergence threshold. The 3D analytical model seems to describe better the experimental set-up, eventhough the experimental critical velocities are consistently higher. This can be surprising, since the strict clamped-clamped conditions are never obtained experimentally; a more realistic description of the boundary conditions would be a pinned-pinned plate, with a high stiffness spring, and this configuration would lead to experimental values smaller than the numerical 3D values. But in this set-up, the plate is slightly stretched to ensure that it is as flat as it can be. This tension, unfortunately not measured, can postpone the onset of divergence. A more realistic approach would be to measure the natural frequencies of the plate *in situ* at zero flow velocity, and modify the parameters in the 3D numerical model (the current geometry is based on the analytical definition of the clamped-clamped natural modes as in [15]).

CONCLUSION

In this work, a numerical 3D-model predicting the onset of divergence instability of a clamped-clamped plate in an axial channel flow has been derived. Results of the model have been compared with experiments and a good aggrement was found. Comparison to analytical and numerical critical velocities obtained when a 2D potential flow is solved enlights the importance of a 3D model for the flow around the structure to correctly pre-

dict the critical velocity.

Future works on this include the complete parametric study of the influence of the channel and plate geometries on the critical velocity and unstable deformations. The collective behavior of a large number of plates will next be addressed.

REFERENCES

[1] Païdoussis, M. P., 1998. *Fluid-structure Interactions Slender Structure and Axial Flows*, Vol. 1. Elsevier.

[2] Païdoussis, M. P., 2006. *Fluid-structure Interactions Slender Structure and Axial Flows*, Vol. 2. Elsevier.

[3] Watanabe, Y., Suzuki, S., Sugihara, M., and Sueoka, Y., 2002. "An experimental study of paper flutter". *Journal of Fluids and Structures,* ***16***(4), pp. 529–542.

[4] Kornecki, A., Dowell, E., and O'Brien, J., 1976. "On the aeroelastic instability of two-dimensional panels in uniform incompressible flow". *Journal of Sound and Vibration,* ***47***(2), pp. 163–178.

[5] Guo, C. Q., and Païdoussis, M. P., 2000. "Analysis of hydroelastic instabilities of rectangular parallel-plate assemblies". *Journal of Pressure Vessel Technology,* ***122***(4), Mar., pp. 502–508.

[6] Modarres-Sadeghi, Y., Païdoussis, M. P., Semler, C., and Grinevich, E., 2008. "Experiments on vertical slender flexible cylinders clamped at both ends and subjected to axial flow". *Philosophical Transactions of the Royal Society A: Mathematical, Physical and Engineering Sciences,* ***366***(1868), pp. 1275–1296.

[7] Doaré, O., Sauzade, M., and Eloy, C., 2011. "Flutter of an elastic plate in a channel flow: Confinement and finite-size effects". *Journal of Fluids and Structures,* ***27***(1), Jan., pp. 76–88.

[8] Doaré, O., Mano, D., and Ludena, J. C. B., 2011. "Effect of spanwise confinement on flag flutter: Experimental measurements". *Physics of Fluids (1994-present),* ***23***(11), p. 111704.

[9] Timoshenko, S., and Woinowsky-Krieger, S., 1959. *Theory of plates and shells*. Mc Graw Hill.

[10] Kim, G., and Davis, D. C., 1995. "Hydrodynamic instabilities in flat-plate-type fuel assemblies". *Nuclear Engineering and Design,* ***158***(1), Sept., pp. 1–17.

[11] Michelin, S., and Llewellyn Smith, S. G., 2009. "Linear stability analysis of coupled parallel flexible plates in an axial flow". *Journal of Fluids and Structures,* ***25***(7), pp. 1136–1157.

[12] Guo, C. Q., and Païdoussis, M., 2000. "Stability of rectangular plates with free side-edges in two-dimensional inviscid channel flow". *Journal of Applied Mechanics,* ***67***(1), pp. 171–176.

[13] Batchelor, G., 1967. *An introduction to fluid dynamics*. Cambridge University Press, Cambridge, UK.

[14] Drazin, P. G., and Reid, W. H., 2004. *Hydrodynamic instability*. Cambridge University Press.

[15] Blevins, R. D., 1984. *Formulas for natural frequency and mode shape*. Krieger.

[16] Geuzaine, C., and Remacle, J., 2009. "Gmsh: a three-dimensional finite element mesh generator with built-in pre- and post-processing facilities". *International Journal for Numerical Methods in Engineering,* ***79***(11), pp. 1309–1331.

[17] *Code_Aster*, http://www.code-aster.org.

[18] Lamb, H., 1932. *Hydrodynamics*. Dover.

[19] Milne-Thomson, L. M., 1996. *Theoretical hydrodynamics*. Dover.

Appendix A: resolution of 2D fluid equations by complex analysis

For the sake of illustration, the ideal case of a flexible plate submitted to a potential flow in two dimensions can be analytically studied. Let L be the plate length in the flow direction, denoted by x, and let the deformation occur in the z direction. Assuming that all variables do not depend on the y coordinate, the fluid flow can be described with the help of complex functions. Let first the half space between the plate and the upper wall be considered, let H be the distance to the upper wall (in m). Classical textbooks [18, 19] describe in details how complex functions can be used to determine solutions of the Laplace equation in two dimensions. More precisely, if F is a function of the complex variable $Z = x + iz$, the real part of F automatically fulfills the Laplace equation, whereas the isovalues of the imaginary part of F are streamlines of the potential flow.

Following the same line of reasoning as in the main sections, it is assumed that the plate deformation generates only a small perturbation of the fluid flow. The complex potential can hence be written as the sum of the unperturbed potential UZ and of a perturbation Φ. Due to mass conservation, the lower streamline coincides with the plate boundary; this condition can be explicitly written for small deformations as the constancy of the imaginary part of $UZ + \Phi$ along $Z = x + i\zeta(x)$. At the first order of the perturbation, it becomes:

$$U\zeta(x) + \mathrm{Im}\left(\Phi(Z = x)\right) = constant \tag{18}$$

a relation equivalent to Eq. (3), yet easier to handle because no space derivative is present. For practical purposes, the constant in Eq. (18) can be chosen equal to zero without loss of generality.

Having in mind that the mode shapes of the plate are combinations of trigonometric and hyperbolic functions, it makes sense to look for a similar expansion of Φ extended to the complex domain. In a manner similar to Eq. (4), the potential is written as

the summation of weighted dimensionless terms φ_n:

$$\Phi = U \sum_n q_n \varphi_n (K_n Z - i K_n D) \tag{19}$$

so that the continuity condition along the plate (18) reduces to:

$$\xi_n(x) = -\mathrm{Im}\left(\varphi_n(K_n x - i K_n D)\right) \tag{20}$$

the term $-iD$ being added to the complex coordinate Z for ensuring that the overall variable inside the function φ_n is real along the upper wall. Provided that φ_n is also real, the upper wall is a streamline and the upper boundary condition is automatically fulfilled.

As shown by Eq. (8), the pressure field generated by the fluid can be determined with the help of the steady Bernoulli equation. At the first order, the perturbed pressure obeys:

$$\frac{p}{\rho} = -U \frac{\partial}{\partial x} \mathrm{Re}\left(\Phi\right) = -U \mathrm{Re}\left(\frac{d\Phi}{dZ}\right) \tag{21}$$

Expanding the potential according to Eq. (19), the dimensionless pressure becomes:

$$\frac{p}{\rho U^2} = -\sum_n K_n q_n \mathrm{Re}\left(\varphi_n'(K_n Z - i K_n D)\right) \tag{22}$$

where φ_n' is the derivative of φ_n along the variable $K_n Z$. Eqs. (19), (20) and (22) summarize the resolution of the fluid equations based on the complex potentials φ_n: for a prescribed mode shape ξ_n, an adequate combination of trigonometric and hyperbolic complex functions builds up the potential φ_n, which can be used to detemine the pressure. This procedure also holds for the half space below the plate, by replacing D by $-D$.

The dimensionless matrix $\mathbf{H}$ can be written:

$$H_{pn} = \frac{K_p L \int \mathrm{Re}(\varphi_p^{+\prime} - \varphi_p^{-\prime}) \xi_n \, ds}{\int \xi_n^2 ds} \tag{23}$$

As an illustration, a clamped-clamped plate of length L exhibits mode shapes defined by [15]

$$\xi_n = \cos(k_n x/L) - \cosh(k_n x/L) - \sigma_n(\sin(k_n x/L) - \sinh(k_n x/L)) \tag{24}$$

k_n being a dimensionless wavenumber fulfilling $\cos k_n \cosh k_n = 1$ and σ_n being equal to $(\cos k_n - \cosh k_n)/(\sin k_n - \sinh k_n)$. The potential φ_n is expanded in terms:

$$\varphi_n = A_n \cos(\tilde{Z}_n) + B_n \cosh(\tilde{Z}_n) + C_n \sin(\tilde{Z}_n) + D_n \sinh(\tilde{Z}_n) \tag{25}$$

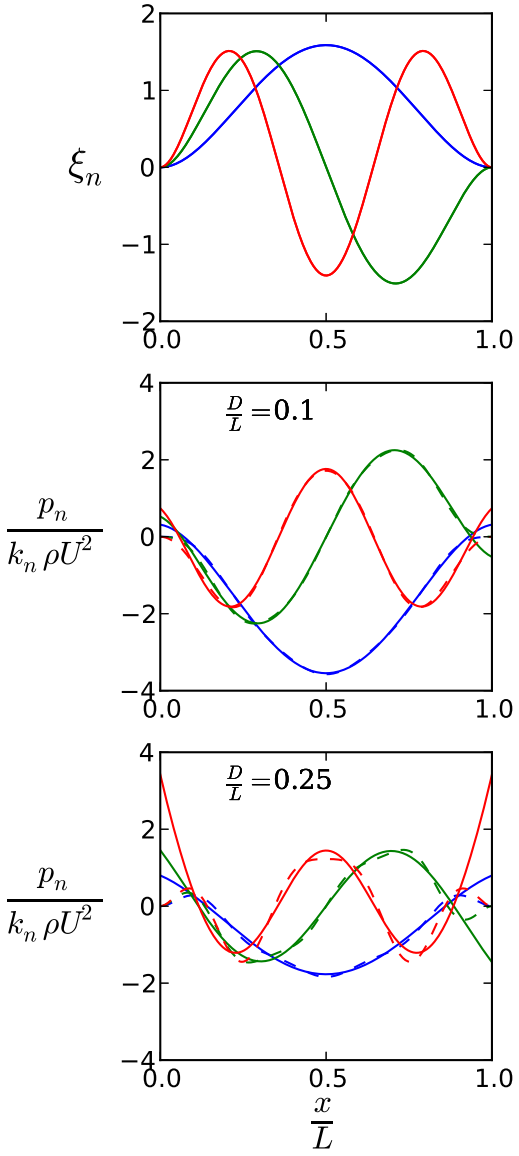

FIGURE 7. COMPARISON OF THE FIRST PLATE MODES (UPPER CURVE) AND OF THE PRESSURE THEY GENERATE (LOWER CURVES) FOR TWO REDUCED WALL-TO-PLANE DISTANCE $\frac{H}{L}$. PLAIN LINE: ANALYTIC SOLUTION, DASHED LINE: MODAL EXPANSION WITH FIVE TERMS.

where $\tilde{Z}_n$ stands for $K_n(Z - iD)$ and where the coefficients A_n, B_n, C_n and D_n are given in [15]. The pressure can be analytically expressed with the same set of coefficients, and the results are illustrated in Fig. 7.